Electronic Supplementary Material (ESI) for Inorganic Chemistry Frontiers.

Electronic Supplementary Information

Metal-free corrole-based donor-acceptor porous organic polymers as efficient bifunctional catalysts for hydrogen evolution and oxygen reduction reactions

Jie Bai[a], Ruichen Li[a], Jiancheng Huang[a], Xuefang Shang[a], Ge Wang[b,c,*], Shujun Chao[a,*]

[a]*Xinxiang Engineering Technology Research Center of Functional Medical Nanomaterials, School of Basic Medical Sciences, Xinxiang Medical University, Xinxiang 453003, P. R. China. E-mail: chaoshujun1979@163.com*

[b]*School of Basic Medical Sciences, Xinxiang Medical University, Xinxiang 453003, P. R. China. E-mail: dongqing1126@163.com*

[c]*The First Affiliated Hospital of Xinxiang Medical University, Xinxiang 453003, P. R. China*

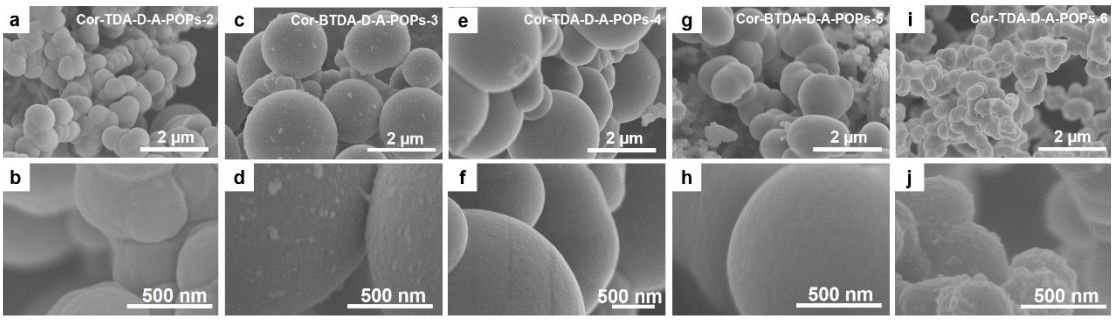

Fig. S1 FESEM images of other five constructed Cor-D-A-POPs.

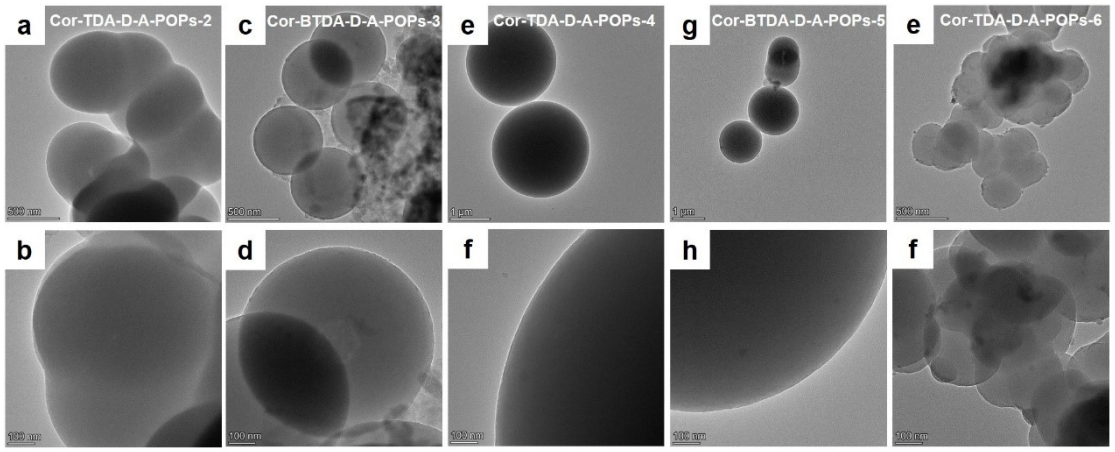

Fig. S2 TEM images of other five constructed Cor-D-A-POPs.

The dipole moments of *n*-butanol, mesitylene, *o*-dichlorobenzene and 1,4-dioxane are 1.66 D, 0.32 D, 2.68 D, and 0.40 D, respectively. When a mixed solvent contained a non-polar solvent of mesitylene and a weak polar solvent of *n*-butanol (1.34 D difference in their dipole moments), Cor-BTDA-D-A-POPs-1 and Cor-TDA-D-A-POPs-2 exhibit rough microspheres regardless of whether the electron donor was BTDA or TDA. When a mixed solvent was composed of a weak polar solvent of *n*-butanol and a strong polar solvent of *o*-dichlorobenzene (1.02 D difference in their dipole moments), Cor-BTDA-D-A-POPs-3 using BTDA donor exhibits rough microspheres, while Cor-TDA-D-A-POPs-4 using TDA donor exhibits smooth microspheres. When a mixed solvent contained two non-polar solvents of mesitylene and 1,4-dioxane (0.08 D difference in their dipole moments), Cor-BTDA-D-A-POPs-5 using BTDA donor exhibits smooth microspheres, while Cor-TDA-D-A-POPs-6 using TDA donor exhibits rough microspheres. The results indicate that if using a weakly polar mixed solvent, the

catalysts will exhibit rough microspheres regardless of using BTDA or TDA donor; if using a strongly polar mixed solvent, the catalyst will exhibit rough microspheres when using BTDA donor; if using a non-polar mixed solvent, the catalyst exhibits rough microspheres when using TDA donor.

DFT computations

The electronic structures for studied molecules (Cor-BTDA-D-A-POPs and Cor-TDA-D-A-POPs) were studied by DFT, where all structures were optimized by the B3LYP functional and def2-SVP basis set by using ORCA 5.0.4[1-4]. The long-range van der Waals (vdW) interactions were handled by Grimme's DFT-D3 scheme[5]. Harmonic vibrational frequency was performed at the same level. HOMO and LUMO were calculated by Multiwfn 3.8 (dev)[6], whose input files were extracted from molden files from ORCA, and plotted by VMD 1.9.3[7].

Computational models

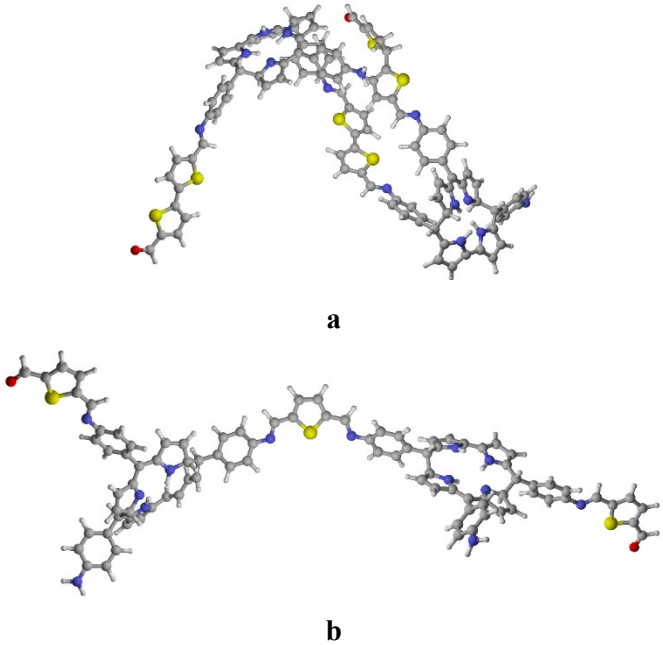

a

b

Fig. S3 The optimized geometries for (a) Cor-BTDA-D-A-POPs and (b) Cor-TDA-D-A-POPs model systems, where the white, gray, blue, red, and yellow balls denote H, C, N, O, and S atoms, respectively.

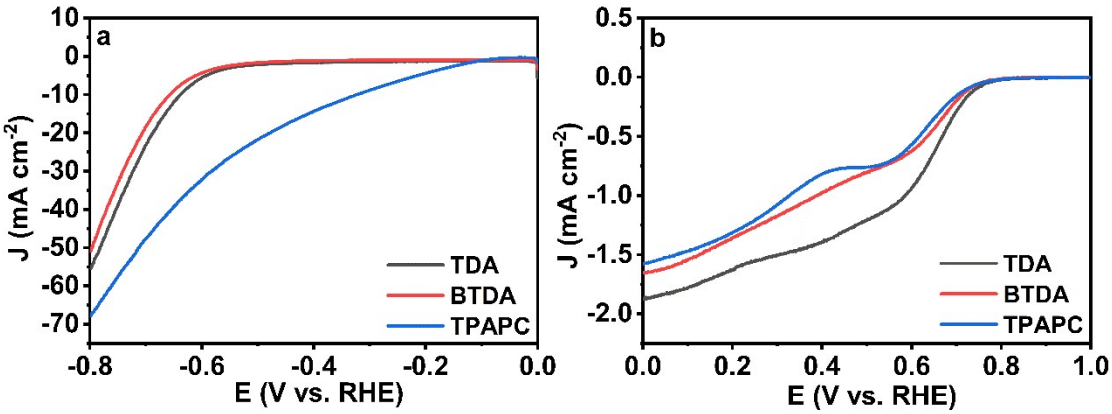

Fig. S4 HER polarization curves (a) and ORR polarization curves (b) of TDA, BTDA and TPAPC.

Table S1. Comparison for HER activity of Cor-BTDA-D-A-POPs-1 with some reported POPs and COFs. The scale for all measured potentials was an RHE.

Materials	**$\eta_{10,HER}$ / mV**	**Tafel slope / mV dec^{-1}**	**R_{ct} / Ω**	**Electrolyte**	**References**
Cor-BTDA-D-A-POPs-1	100	83.6	22.7	1 M KOH	This work
CoNPs@JUC-625	146	186.0	14.9	1 M KOH	8
JLNU-COFs-302	91	103.4	154	1 M KOH	9
NiTAPP-NiACQ	117		60	1 M KOH	10
c-CNT-0.68@TpBpy-Ru	112	160.0	33.7	1 M KOH	11
JLNU-300	290	99.0	153	1 M KOH	12
PyTTA-BPyDCA COF film	315	107	31.5	0.5 M H_2SO_4	13
Cu-TTP	115	98	31.53	0.5 M H_2SO_4	14
TpPAM	250	106	90.34	0.5 M H_2SO_4	15

Table S2. Comparison for ORR activity of Cor-BTDA-D-A-POPs-1 with some reported POPs and COFs. The scale for all measured potentials was an RHE.

Materials	E_O / V	$E_{1/2}$ / V	**Tafel slope / mV dec^{-1}**	**References**
Cor-BTDA-D-A-POPs-1	0.81	0.66	90.0	This work
C-COF	0.86	0.73	144.0	16
C-Fe-COF	0.73	0.55	-	
TBPA-phen	0.80	-	56.0	17
H_3-POP	-	0.71	90.0	18
JUC-527	0.78	0.63	72.3	19
JUC-608	0.8	0.72	85.0	20
BUCT-COF-1/CNT	-	0.68	49.1	21
Py-TD-COF	0.83	0.70	252	22
H-TP-COF	0.71	0.65	104	23
TFPB-TAPB-COF	-	0.65	90.3	24

All fragment structures of Cor-BTDA-D-A-POPs and Cor-TDA-D-A-POPs and reaction intermediates of HER and ORR were all optimized under the framework of DFT with B3LYP functional and 6-31g(d) basis set[25-29]. To describe the solvation effect, the SMD (Solvation Model Based on Density) implicit solvent model was used in all calculations[30]. The DFT-D3 dispersion correction method was also used in these calculations. The vibrational frequency analysis was carried out for the optimized structures with the same calculation method to obtain the zero-point energy and free energy corrections. The thermodynamic correction terms and Gibbs free energy of the structures at 298.15 K were then obtained using Shermo program[31]. In order to obtain the electron energy with higher accuracy which has the major impact on the accuracy of Gibbs free energy, single point calculations for the optimized structures with M06-2x functional[32] and 6-311G(d,p) basis set were performed. Finally, the single point energy was added to the free energy correction calculated before to obtain the Gibbs free energy. All these

DFT calculations were performed using Gaussian 16 program suite[33]. The energy of electron could not be calculated directly. Therefore, the indirect method of computational hydrogen electrode[34] was applied to calculate the Gibbs free energy change of each electrochemical reaction step.

The HER proceeds in two steps: (a) adsorption of hydrogen on the catalytic site ($H^+ + e^- + *$), and (b) release of dihydrogen molecule ($1/2H_2 + *$), where * represents the catalytic site. The Gibbs free energy of hydrogen absorption (ΔG_{H*}) can be calculated from the following equation:

$$\Delta G_{H*} = E_{H*} - E_* - 0.5 E_{H_2} + \Delta E_{ZPE} - T\Delta S$$

where E_{H*}, E_*, E_{H_2}, ΔE_{ZPE}, T and ΔS represent the energy of catalyst with hydrogen absorption, the energy of catalyst, the energy of H_2, the difference between zero-point vibrational energy of H_2 and catalyst with hydrogen absorption, temperature and the entropy change (ΔS) of the system, respectively.

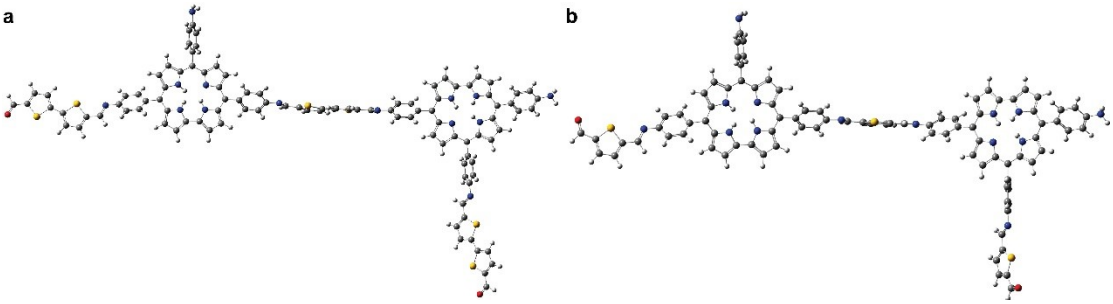

Fig. S5 Optimized BTDA-TPAPC (a) and TDA-TPAPC (c) structural units.

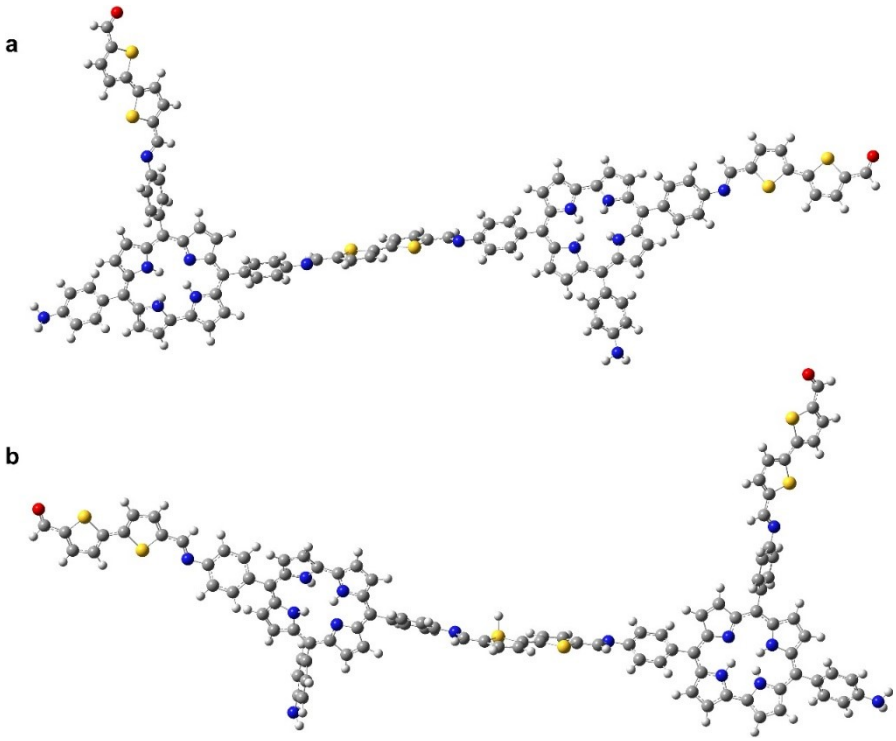

Fig. S6 The optimized geometry structures of H* on Cor-BTDA-D-A-POPs at the pyrrolic-N site (a) and thiophene-S site (b).

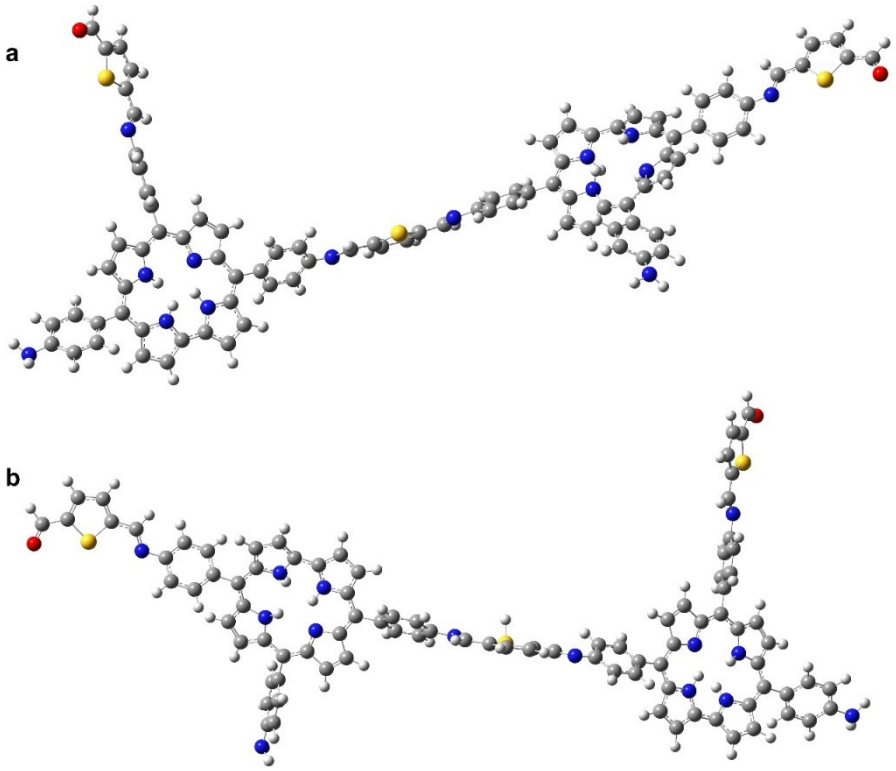

Fig. S7 The optimized geometry structures of H* on Cor-TDA-D-A-POPs at the pyrrolic-N site (a) and thiophene-S site (b).

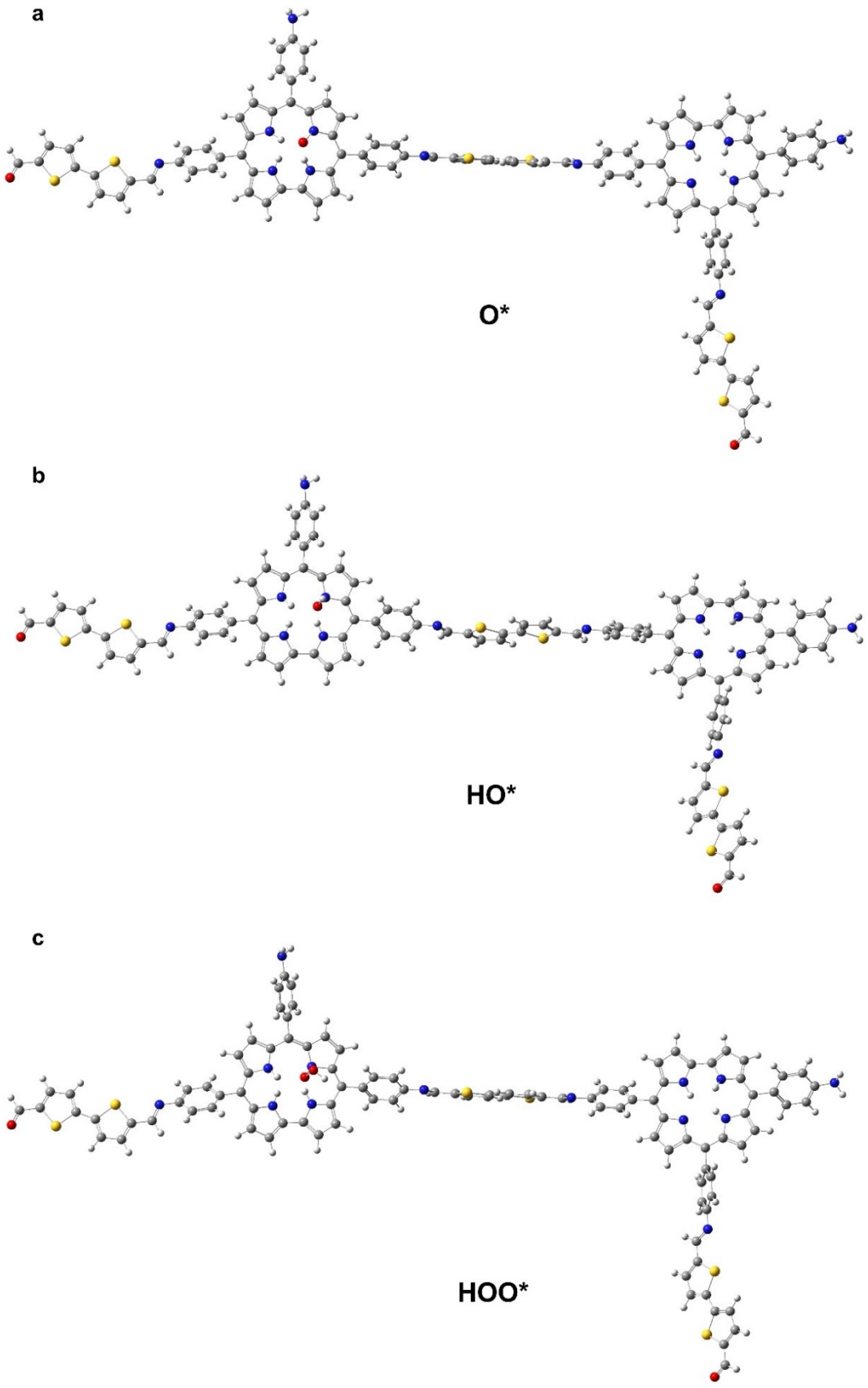

Fig. S8 The optimized geometry structures of all possible intermediates on Cor-BTDA-D-A-POPs (a-c) at the pyrrolic-N site.

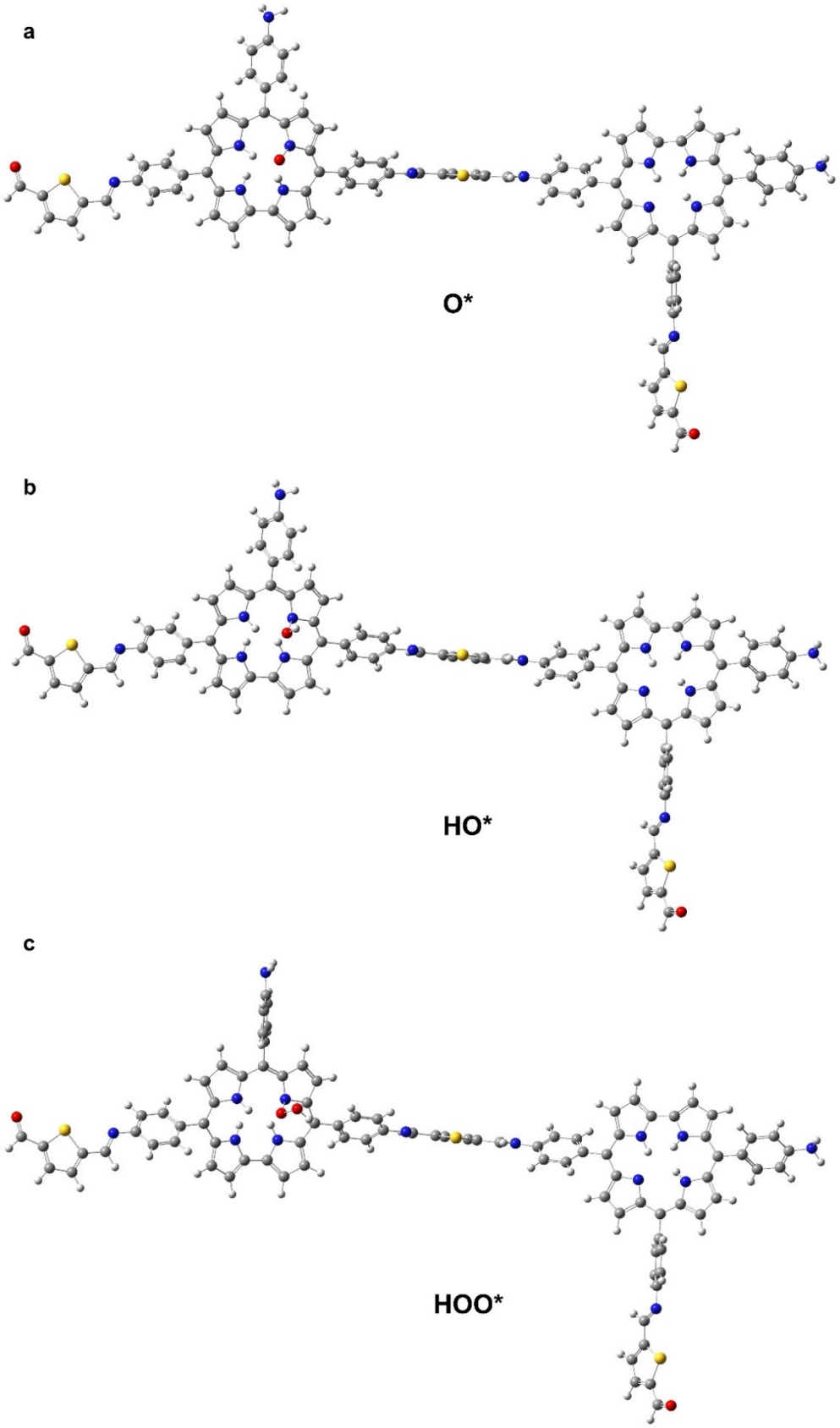

Fig. S9 The optimized geometry structures of all possible intermediates on Cor-TDA-D-A-POPs (a-c) at the pyrrolic-N site.

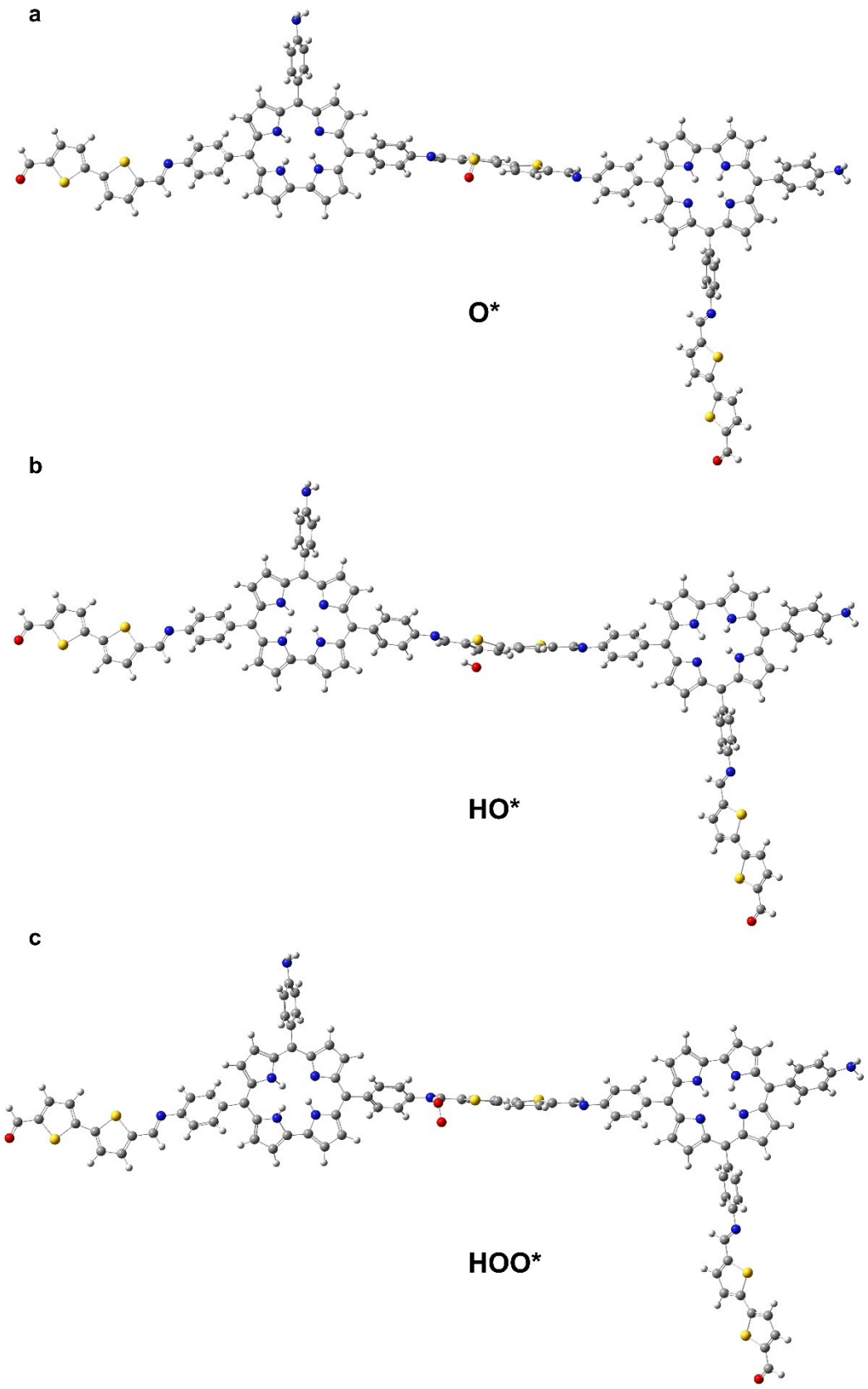

Fig. S10 The optimized geometry structures of all possible intermediates on Cor-BTDA-D-A-POPs (a-c) at the thiophene-S site.

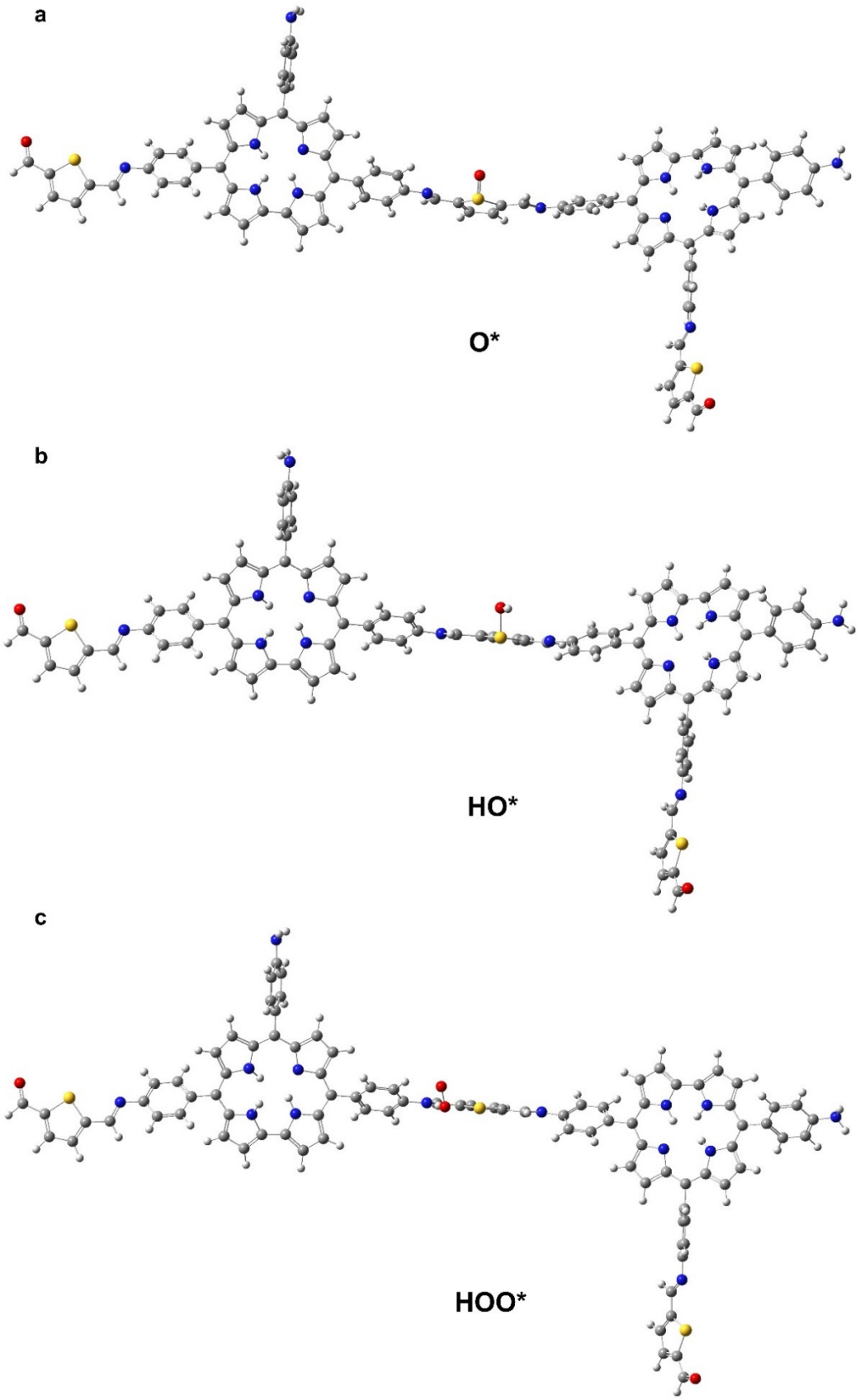

Fig. S11 The optimized geometry structures of all possible intermediates on Cor-TDA-D-A-POPs (a-c) at the thiophene-S site.

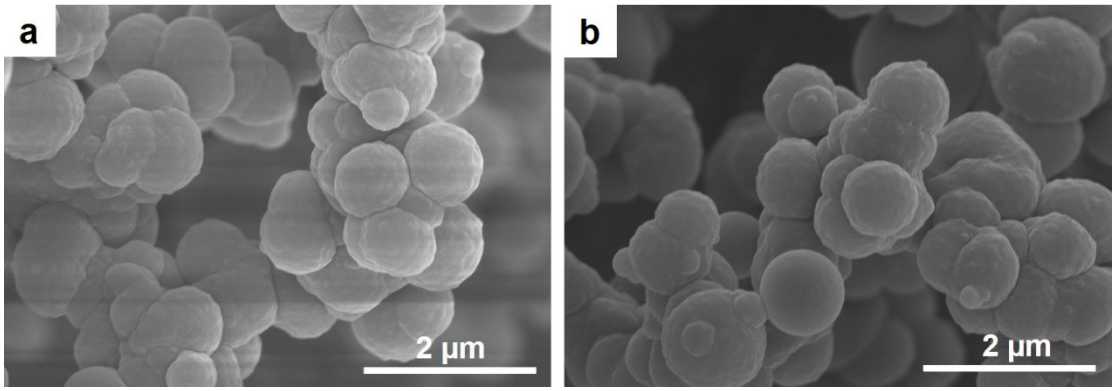

Fig. S12 FESEM images of Cor-BTDA-D-A-POPs-1 after HER (a) and ORR (b) stability tests.

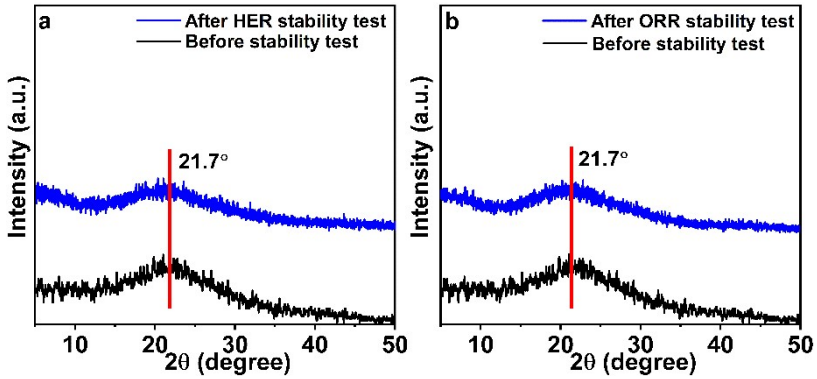

Fig. S13 XRD patterns of Cor-BTDA-D-A-POPs-1 before and after HER (a) and ORR (b) stability tests.

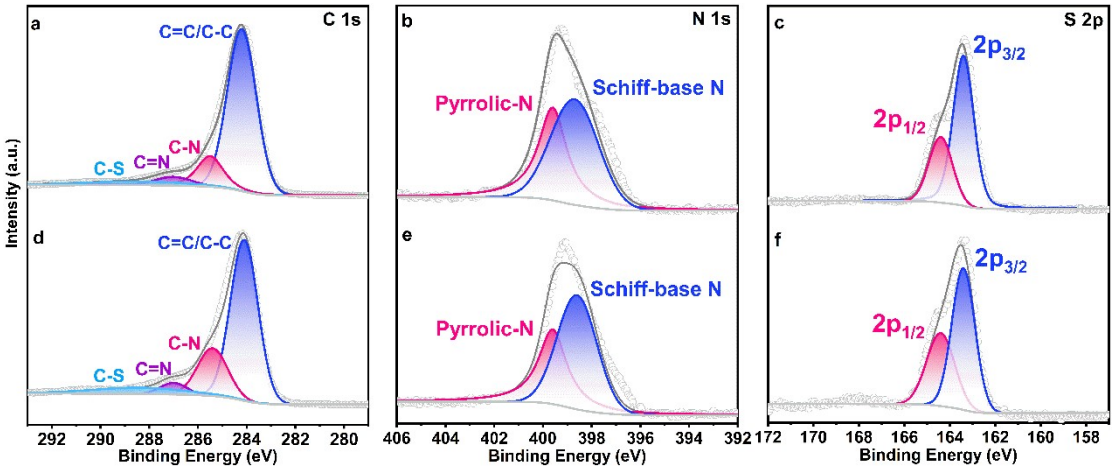

Fig. S14 High-resolution C 1s (a and d), N 1s (b and e) and S 2p (c and f) XPS spectra of Cor-BTDA-D-A-POPs-1 after HER and ORR stability tests.

The C 1s spectra of Cor-BTDA-D-A-POPs-1 (Fig. S14a and d) after HER/ORR stability tests display four peaks at 284.1 (284.2), 285.5, 287.0 and 288.4 eV, which can be attributed to C-C/C=C, C-N, C=N and C-S bonds, respectively. In the N 1s spectra (Fig. S 14b and e) after HER/ORR stability tests, two peaks at 398.7 and 399.6 eV can be assigned to Schiff-base N and pyrrolic-N species, respectively. Its S 2p spectra (Fig. S14c and f) can be deconvoluted into S $2p_{3/2}$ region (163.4 eV) and S $2p_{1/2}$ region (164.4 eV) of thiophene-S species after HER/ORR stability tests.

References:

1 C. Adamo and V. Barone, Toward reliable density functional methods without adjustable parameters: the PBE0 model, *J. Chem. Phys.*, 1999, **110**, 6158-6169.

2 F. Weigend and R. Ahlrichs, Balanced basis sets of split valence, triple zeta valence and quadruple zeta valence quality for H to Rn: design and assessment of accuracy, *Phys. Chem. Chem. Phys.*, 2005, **7**, 3297-3305.

3 F. Weigend, Accurate coulomb-fitting basis sets for H to Rn, *Phys. Chem. Chem. Phys.*, 2006, **8**, 1057-1065.

4 F. Neese, The ORCA program system, *WIRES Comput. Mol. Sci.*, 2012, **2**, 73-78.

5 S. Grimme, S. Ehrlich and L. Goerigk, Effect of the damping function in dispersion corrected density functional theory, *J. Comput. Chem.*, 2011, **32**, 1456-1465.

6 T. Lu and F. Chen, Multiwfn: a multifunctional wavefunction analyzer, *J. Comput. Chem.*, 2012, **33**, 580-592.

7 W. Humphrey, A. Dalke and K. Schulten, VMD: Visual molecular dynamics, *J. Mol. Graph.*, 1996, **14**, 33-38.

8 J. Song, L. Liao, Z. Zhang, Y. Yusran, R. Wang, J. Fang, Y. Liu, Y. Hou, Y. Wang and Q. Fang, 2D microporous covalent organic frameworks as cobalt nanoparticle supports for electrocatalytic hydrogen evolution reaction, *Crystals*, 2022, **12**, 12070880.

9 Y. Ma, Y. Fu, W. Jiang, Y. Wu, C. Liu, G. Che and Q. Fang, Excellent electrocatalytic performance of metal-free thiophene-sulfur covalent organic frameworks for hydrogen evolution in alkaline medium, *J. Mater. Chem. A*, 2022, **10**, 10092-10097.

10 A. Wang, X. Yang, Q. Wang, Y. Dou, L. Zhao, W. Zhu, W. Zhao and G. Zhu, Acenaphthenediimine complex-bridged porphyrin porous organic polymer with enriched active sites as a robust water splitting electrocatalyst, *J. Colloid Interface Sci.*, 2024, **657**, 748-756.

11 X. Sun, Y. Hu, Y. Fu, J. Yang, D. Song, B. Li, W. Xu and N. Wang, Single Ru sites on covalent organic framework-coated carbon nanotubes for highly efficient electrocatalytic hydrogen evolution, *Small*, 2023, **20**, 2305978.

12 Y. Ma, Y. Fu, Y. Han, J. Li, W. Jiang, Y. Lu, C. Liu, G. Che and B. Hu, A sulfur-containing two-dimensional covalent organic framework with electrocatalytic hydrogen evolution in alkaline medium, *CrystEngComm*, 2022, **24**, 7447-7453.

13 M. Liu, Y. Liu, J. Dong, Y. Bai, W. Gao, S. Shang, X. Wang, J. Kuang, C. Du, Y. Zou, J. Chen and Y. Liu, Two-dimensional covalent organic framework films prepared on various substrates through vapor induced conversion, *Nature Comm.*, 2022, **13**, 1411.

14 V. Rajagopal, M. Manivannan, M. Kathiresan, V. Suryanarayanan and L. A. Jones, Metal/metal oxide-decorated covalent organic frameworks as electrocatalysts for electrocarboxylation and water splitting, *Mater. Chem. Phys.*, 2022, **285**, 126104.

15 B. C. Patra, S. Khilari, R. N. Manna, S. Mondal, D. Pradhan, A. Pradhan and A. Bhaumik, A metal-free covalent organic polymer for electrocatalytic hydrogen evolution, *ACS Catal.*, 2017, **7**, 6120−6127

16 D. Wu, Q. Xu, J. Qian, X. Li and Y. Sun, Bimetallic covalent organic frameworks for constructing multifunctional electrocatalyst, *Chem. Eur. J.*, 2019, **25**, 3105-3111.

17 S. Singh, M. K. Ghorai and K. K. Kar, A cobalt harnessed phenanthroline and triphenylamine-based conjugated mesoporous polymer designed by a donor-acceptor approach for trifunctional electrocatalysis, *J. Mater. Chem. A*, 2023, **11**, 20290-20301.

18 H. Lei, Q. Zhang, Z. Liang, H. Guo, Y. Wang, H. Lv, X. Li, W. Zhang, U. P. Apfel and R. Cao, Metal-corrole-based porous organic polymers for electrocatalytic oxygen reduction and evolution reactions, *Angew. Chem. Int. Ed.*, 2022, **61**, 202201104.

19 D. Li, C. Li, L. Zhang, H. Li, L. Zhu, D. Yang, Q. Fang, S. Qiu and X. Yao, Metal-free thiophene-sulfur covalent organic frameworks: precise and controllable synthesis of catalytic active sites for oxygen reduction, *J. Am. Chem. Soc.*, 2020, **142**, 8104-8108.

20 S. Chang, C. Li, H. Li, L. Zhu and Q. Fang, Stable thiophene-sulfur covalent organic frameworks for oxygen reduction reaction (ORR), *Chem. Res. Chin. Univ.*, 2022, **38**, 396-401.

21 R. Bao, Z. Xiang, Z. Qiao, Y. Yang, Y. Zhang, D. Cao and S. Wang, Designing thiophene-enriched fully conjugated 3D covalent organic framework as metal-free oxygen reduction catalyst for hydrogen fuel cells, *Angew. Chem. Int. Ed.*, 2022, **62**, 202216751.

22 S. Huang, B. Zhang, D. Wu, Y. Xu, H. Hu, F. Duan, H. Zhu, M. Du and S. Lu, Linkage engineering in covalent organic frameworks as metal-free oxygen reduction electrocatalysts for hydrogen peroxide production, *Appl. Catal. B Environ. Angew. Chem. Int. Ed.*, 2024, **340**, 123216.

23 J. Y. Yue, Y. T. Wang, X. Wu, P. Yang, Y. Ma, X. H. Liu and B. Tang, Two-dimensional porphyrin covalent organic frameworks with tunable catalytic active sites for the oxygen reduction reaction, *Chem. Comm.*, 2021, **57**, 12619.

24 G. Jiang, L. Zhang, W. Zou, W. Zhang, X. Wang, H. Song, Z. Cui and L. Du, Precise and controllable tandem strategy triggering boosted oxygen reduction activity, *Chin. J. Catal.*, 2022, **43**, 1042-1048.

25 A. D. Becke, Density-functional exchange-energy approximation with correct asymptotic behavior, *Chin. J. Catal.*, 1988, **38**, 3098-3100.

26 C. Lee, W. Yang and R. G. Parr, Development of the colle-salvetti correlation-energy formula into a functional of the electron density, *Phys. Rev. B*, 1988, **37**, 785-789.

27 A. D. Becke, Density-functional thermochemistry. III. The role of exact exchange, *J. Chem. Phys.*, 1993, **98**, 5648-5652.

28 G. A. Petersson, A. Bennett, T. G. Tensfeldt, M. A. Al-Laham, W. A. Shirley and J. Mantzaris, A complete basis set model chemistry. I. The total energies of closed-shell atoms and hydrides of the first-row elements, *J. Chem. Phys.*, 1988, **89**, 2193-2218.

29 G. A. Petersson and M. A. AI-Laham, A complete basis set model chemistry. II. Open-shell systems and the total energies of the first-row atoms, *J. Chem. Phys.*, 1991, **94**, 460447.

30 A.V. Marenich, C. J. Cramer and D. G. Truhlar, Universal solvation model based on solute electron density and on a continuum model of the solvent defined by the bulk dielectric constant and atomic surface tensions, *J. Phys. Chem. B*, 2009, **113**, 6378-6396.

31 T. Lu and Q. Chen, Shermo: a general code for calculating molecular thermochemistry properties, *Comput. Theor. Chem.*, 2021, **1200**, 113249.

32 Y. Zhao and D. G. Truhlar, The M06 suite of density functionals for main group thermochemistry, thermochemical kinetics, noncovalent interactions, excited states, and transition elements: two new functionals and systematic testing of four M06-class functionals and 12 other functionals, *Theor. Chem. Acc.*, 2007, **120**, 215-241.

33 M. J. Frisch, G. W. Trucks, H. B. Schlegel, G. E. Scuseria, M. A. Robb, J. R. Cheeseman, G. Scalmani, V. Barone, G. A. Petersson and H. Nakatsuji. Gaussian 16, Revision B.01, 2016, {Gaussian}, Inc., Wallingford CT (2016).

34 A. A. Peterson, F. Abild-Pedersen, F. Studt, J. Rossmeisl and J. K. Nørskov, How copper catalyzes the electroreduction of carbon dioxide into hydrocarbon fuels, *Environ. Sci. Technol.*, 2010, **3**, 1311-1315.